Photocatalytic ceramic membrane: Effect of the illumination intensity and distribution

Shuyana A. Heredia Deba [a,b], Bas A. Wols [a,c], Doekle R. Yntema [a], Rob G.H. Lammertink [b,*]

[a] *Wetsus European Center of Excellence for Sustainable Water Technology, 8911MA Leeuwarden, The Netherlands*
[b] *Membrane Science and Technology, Faculty of Science and Technology (TNW), University of Twente, Drienerlolaan 5, 7522 NB Enschede, The Netherlands*
[c] *KWR Watercycle Research Institute, 3430 BB, Nieuwegein, The Netherlands*

ARTICLE INFO

ABSTRACT

The principles and application of heterogeneous photocatalytic processes have gained wide attention, especially to the effectiveness of the process. In this work a mono and a multi-LED lamp are used to study the impact of the UV light intensity and distribution on the semiconductor surface during the degradation of organic compounds in water. A well-defined scan of the electromagnetic radiation profile on the surface of the membrane was obtained and evaluated. Comparing two lamp configurations with a total photon flux of 210 W.m^{-2} and using a filtration rate of 9.7 L.m^{-2}.h^{-1}, resulted in 20 % more degradation for the most homogeneous light distribution. Furthermore, the reaction rate relation to the photon flux was also studied, with a surface reaction model that includes possible mass transfer limitations. The surface reaction constant increased linearly with the irradiation intensity for the complete studied range [50 to 550 W.m^{-2}] for the most homogeneous illumination distribution. A less uniform distribution resulted in a less than proportional reaction rate constant with respect to the incident photon flux between 100 and 210 W.m^{-2}. This work adds valuable information to the photocatalysis field to improve the light efficiency in a photoreactor to enhance the degradation of pollutants.

1. Introduction

Heterogeneous photocatalysis principles and their potential applications have been investigated in depth over the last 25 years. According to Scopus, over 8000 papers were published in 2021 alone with the word "photocatalysis" in the title, abstract, or as keywords. However, several challenges are still to be solved, such as mass transfer limitations, nature of the intermediate products during the degradation, catalysis deactivation, photon transfer limitations, or low quantum efficiency, among others [1,2]. Various reactor designs and operational conditions have been proposed to overcome some of the current limitations next to catalyst material design and modification.

Significant research in the field is focused on improving the light efficiency for photocatalytic reactions by improving the material characteristics to absorb light at larger wavelengths in the solar radiation spectrum [3] (i.e., band gap engineering such as doping [4, 5], heterojunction [6,7], or photosensitization [8], among others), or by investigating different light sources [9,10]. These investigations have led to significant advancement regarding photon usage efficiency and widened the applicability of photocatalysis. Less attention has gone to another essential aspect of the photoreactor: the illumination distribution.

In a photocatalytic reaction, electromagnetic radiation is the only source of energy to activate the photocatalyst. The photocatalyst absorbs photons to excite valence band electrons onto the conduction band which results in highly active photo-generated holes (h$^+$) in the valence band and photo-generated electrons (e$^-$) in the conduction band [11,12]. The photo-generated h$^+$ and e$^-$ can diffuse to the semiconductor surface to generate reactive oxygen active species (O$_2^-$, OH$^-$, H$_2$O$_2$, etc.), that can degrade organic molecules. The irradiation intensity directly affects the number of photons available to the photocatalyst and determines the number of electron–hole pairs and reactive species produced [13] until the photon saturation is reached, i.e., until the maximum number of electron–hole pairs is generated. Each type of photocatalyst absorbs light at different wavelengths, as the energy band gap directly determines the excitation wavelengths of the photocatalyst. For titanium dioxide, a widely used semiconductor photocatalyst, the energy gap is dependent on its crystalline structure, where it is 3.2 eV for anatase, 3.03 eV for rutile, and 3.30 eV for brookite. An energy equal to or greater than the band gap is needed to excite the electron which corresponds to radiation wavelengths of 388 nm for anatase, 410 nm for rutile, and 376 nm for brookite.

---

* Corresponding author.
  E-mail address: r.g.h.lammertink@utwente.nl (R.G.H. Lammertink).

Significant research focus concerns the relation between photon flux and degradation kinetics of specific compounds. The apparent reaction rate constant can be related to the light intensity by the power-law expression $k = \alpha I^\beta$ where α is a proportionality constant and β is the reaction order with respect to the incident photon flux, I [14]. The general consensus is that the exponent β reduces from 1 to 0.5 when going from low to intermediate light intensities [13,15,16]. This change is attributed to the electron–hole formation rate, which increases more than the photocatalytic degradation rate at higher light intensities and promotes the electron–hole recombination [17]. Most of these studies are done for reactors where the catalyst is present in slurry and agree on a reaction rate constant becoming proportional to the square root of light intensity above ~250 W.m^{-2} [16,18]. Meanwhile, at even higher intensities, the degradation rate becomes independent of the light intensity, i.e., β reduces further from 0.5 to 0. since more incident photons will not produce more electron–hole pairs [19].

Different parameters have been reported in studies on immobilized TiO$_2$ that influence the reaction order with respect to the incident photon flux. Aguado et al. [20] tested three different colloidal suspensions of titania immobilized on a Pyrex support for the decomposition of formic acid. The amount of titania deposited (layer thickness) and the density of the layer depend on the precursor colloid. They found that the exponential relation between the reaction rate constant and the irradiation intensity varied between films with exponents of 0.78 ± 0.20, 0.53 ± 0.14 and 0.60 ± 0.22 for irradiation power densities from 9.25 to 18.5 W.m^{-2}, suggesting that the rate transition may be influenced by the catalyst morphology. Wang et al. [21] studied the effect of radiation intensity on the degradation of dimethyl sulfide using four wavelengths (365, 375, 385, and 402 nm) in a gas flow-through channel with a thin film of immobilized TiO$_2$. For the experiments with the 365 and 375 nm LED lamps the rate transition from linear to a square root was estimated between 5 and 10 W.m^{-2}. While the experiments with the 385 and 402 nm LED lamps did not show such a transition in the studied range from 5 to 25 W.m^{-2}, indicating that the rate transition may also depend on the energy of the irradiated photons. Vesborg et al. [22] investigated the photocatalytic oxidation of CO over TiO$_2$ thin films and found an exponential relation between the reaction rate and the irradiation intensity with an exponent of 0.84 ± 0.03 for irradiation power densities from 1 to 6450 W.m^{-2}. They discuss other articles with similar results where it is considered to be in the "transition region", between the recombination domain and the light limited domain. Due to the wide range of light intensities reported, they find it difficult to conclude that the turnover for CO oxidation can be proportional to incident flux. This shows that not all the configurations have a clear transition through the different regions. Visan et al. [23] investigated the degradation kinetics of cortisone acetate in a microreactor with a TiO$_2$ immobilized porous layer and modeled this to reaction and diffusion kinetics inside this layer. They explained the reaction order change from $\beta = 1$ to 0.5 with respect to the incident photon flux usually found in literature (above ~250 W.m^{-2}) with the prevailing of diffusion during reactions with high intensities. Since at low intensities, the reaction rate is the limiting step and mass transfer limitations can be neglected. Timmerhuis et al. [24] support these findings by comparing two models, with and without mass transfer limitations, to calculate the reaction rate constant for varying light intensities in a microreactor. It was shown that neglecting the mass transfer limitations can lead to lower apparent reaction rate constants at higher photon fluxes. Visan et al. [23] and Timmerhuis et al. [24] reported a reaction order, β, of 1 for a range of light intensities from 55 to 270 W.m^{-2} and from 10 to 2300 W.m^{-2} respectively, showing that the reported rate transition may depend also on the inclusion of mass transport limitations [25].

Compared to the light intensity, much less attention has gone to the illumination distribution effect. The spatial irradiation distribution, intensity, and wavelength used are very diverse in literature, and the lack of knowledge of the radiation field distribution in a photoreactor can lead to erroneous conclusions in photocatalytic processes. Photocatalytic slurry reactors introduce light scattering besides absorption that result in inhomogeneous light distribution, and consequently less optimal efficiency of the photocatalyst. Martín Somers et al. [26] compared the efficiency of two different UV-A sources (mercury fluorescent lamp and 8 or 40 LED-based system) in the photocatalytic degradation of methanol by modeling the light distribution inside an annular slurry reactor and concluded that the improvement in the UV light distribution results in a significant increase in the overall photonic efficiency of the reactor. Casado et al. [2] considered the importance of the radiation field and modeled the effect of different configurations of LED systems on the irradiation distribution. The most homogeneous irradiation profile configuration was used as a slurry reactor for the degradation of cinnamic acid. They showed that the optical thickness affects the rate transition, by investigating different slurry concentrations.

In immobilized photocatalytic reactors, the light distribution is typically more homogeneous as interface scattering due to roughness can be neglected and bulk scattering is not relevant due to absorption. Khodadadian et al. [27] modeled an annular LED-based reactor with the photocatalyst immobilized on the wall for the degradation of toluene in the gas phase. They tested six configurations and found that a non-uniform irradiation distribution on the catalyst surface decreased the recombination of electron–hole pairs. These results are expected because they considered the reaction order to scale with the square root of the incident photon flux, i.e. they were working at irradiation intensities where the recombination rate limits the process. In less irradiated regions of a non-uniform irradiation pattern the intensities will be lower, and hence these areas may be in the light limited domain with less recombination.

This study uses a single-pass dead-end membrane reactor to analyze the spatial radiation implications in the photocatalytic degradation of organic molecules in water using a photocatalytic ceramic membrane. The radiation profile on the membrane surface has been experimentally obtained. The degradation rate using either mono (non-uniform) or multi-LED (uniform) lamps is compared for different irradiation intensities (from 50 to 210 W.m^{-2}). Furthermore, a 1D transport and surface reaction model described previously [28], that includes advection and diffusion transport, is used to obtain the surface reaction rate constants for the two illumination distributions for a range between 50 to 550 W.m^{-2}. This work shows the importance of the spatial radiation, as for the same total irradiation, the degradation will vary with the illumination distribution.

2. Materials and methods

2.1. Experimental setup

Photocatalytic membranes were tested in a flow-through single-pass photocatalytic membrane reactor (PMR) with two different UV-Light Emitting Diode (LED) lamps. A mono-LED lamp (NCSU276AT) was placed 67 mm away from the membrane surface, with an additional lens (AL-12M-119) used to narrow the light distribution angle to 8 degrees. And a multi-LED lamp with 12 LEDs (SBM-120-UV-F34-L405-22) was set at 53 mm from the membrane surface as the distribution was more homogeneous, and at a shorter distance less power is lost. The LEDs were connected to a stabilized DC power supply (Delta electronics), keeping a constant current. The UV radiation was determined using a power meter (Thorlabs) with a Thermal Power Sensor Head (S310-C). The average intensity across the membrane was controlled to ensure that both lamps provided the desired average intensity independently of the distance between the membrane and the lamp. The distribution of light intensity on the membrane surface was measured with a 3D scanning photometer and the spectrum with a fiber optic spectrometer (AvaSpec-3648). The setup was placed inside a cupboard to protect the reactants from the ambient light (see Heredia Deba et al. [28] for details on the setup configuration and the PMR).

2.2. Photocatalytic degradation experiments

Dead-end filtration and degradation experiments were carried out using methylene blue solution (MB) (BOOM, CAS 61-73-4), $C_{16}H_{18}ClN_3S$, as an azo-dye model compound. An aqueous solution of 4 mg L^{-1} of MB dissolved in water containing 1.0 mM sodium sulphate was pumped into the setup with fluxes of 1.6, 3.3, 6.5, 9.7, 13.0, and 16.2 L m^{-2} h^{-1}. These fluxes are in the ranges used in commercial nanofiltration. Sodium sulphate anhydrous (VWR chemicals, CAS 7757-82-6), Na_2SO_4, was used to avoid corrosion in the system which may happen with ultrapure water. Five UV light intensities were evaluated: 50, 100, 210, 350, and 550 W.m^{-2}. The experiments were repeated twice as the reproducibility of the experiments was found to be high. The natural pH and temperature in the reactor were used without further adjustment. A thermal imaging camera (FLIR ONE PRO), with a temperature range from 253.15 K to 393.15 K, was used to measure the temperature distribution during the experiments, see Appendix A.

The discoloration of MB was continuously monitored by passing the permeate through an optical flow cell (FIA-Z-SMA-ML-PE flow cell, 10 mm path length) connected to a UV–Vis spectrometer (Flame Model Spectrometer with Sony Detector, Ocean Optics). The monitored wavelength was 664 nm, corresponding to the maximum absorption peak of MB, see Appendix B for the full spectrum. Prior to the experiment, the membranes were equilibrated with the feed solution to ensure that the discoloration measurements were caused by the photocatalytic reaction and not by the adsorption on the membrane surface. After equilibrating (c.a. 2 h), when the permeate concentration recorded by a UV–Vis spectrometer measured a steady value, the lamp was turned on. The experiment was concluded when the outlet absorbance reached a steady value for each filtration rate.

Two photocatalytic membranes with the same characteristics were used for the experiments, from here on named A and B. In order to compare the photocatalytic properties of both membranes the experiments at 210 W.m^{-2} were reproduced and the data confirmed that the performance of both membranes was similar. More information about the membrane fabrication can be found in our previous work [28], as we used the same titanium dioxide suspension (a mixture of anatase, 80–90%, and rutile VP Disp. W 2730 X from Evonik), deposition technique (dip-coating), and support (γ–alumina interlayer on a α–alumina support). For the experiments with membrane B and the multi-LED lamp one flux, 9.7 L.m^{-2}.h^{-1}, was studied. The membranes were cleaned by calcination for 2 h at 500 °C, where the heating and cooling rates were kept at 2 °C min^{-1}, and reused.

2.3. 1D transport and surface reaction model and diffusion coefficient

A simple 1D transport and surface reaction model was used to analyze the experimental results. Detailed information about the model can be found in [28]. This model is based on the convection–diffusion equation, with a constant inlet concentration and a reaction on the membrane surface as boundary conditions. The solution of the ordinary differential equation with the above-mentioned boundary conditions reads for the permeate concentration to feed concentration ratio:

$$\frac{c_p}{c_b} = \frac{e^{Pe}Pe}{e^{Pe}\left(Pe + Da_{II}\right) - Da_{II}} \tag{1}$$

where two dimensionless numbers are used to calculate the permeate to feed concentration ratio (c_p/c_b): Pe represents the Péclet number, Pe $= uL/D$, with linear velocity u [m s^{-1}], liquid reservoir height L [m], and diffusivity D [m^2 s^{-1}]. Da$_{II} = k'L/D$ is the second Damköhler number, with surface reaction rate constant k' [m s^{-1}]. Experimental permeate concentrations were obtained at different feed flows (Pe) such that Da$_{II}$ was obtained by least squared fitting to the analytical model.

3. Results and discussion

3.1. Lamp characterization

A mono and a multi-LED lamp were used to investigate the methylene blue discoloration under different irradiation conditions. The light distribution on the surface of the membrane is an essential parameter for the photonic efficiency of the system. Fig. 1 depicts the measured power distribution of both lamps at 210 W.m^{-2} overall intensity and the multi-LED at 550 W.m^{-2}. In the scan with the multi-LED lamp, it is worth noting the peripheral wall reflectivity effect in the intensity distribution, this is more visible in the scan at 550 W.m^{-2}, see Fig. 1(e).

The mono-LED lamp produces an inhomogeneous distribution with increased intensity in the middle of the membrane. In contrast, the light distribution from the multi-LED lamp is more homogeneous. Both distributions can be evaluated by the incident radiation uniformity index. This index quantifies the local variations compared to the irradiated area mean value [29]. An index value of 1.0 indicates complete uniformity. The incident radiation uniformity index was 0.74 for the mono-LED lamp and 0.97 for the multi-LED lamp, confirming the more uniform light distribution obtained from the lamp with 12 LEDs. Different incident radiations were measured without a significant effect on the radiation uniformity index on the membrane surface. The black circumference in Fig. 1 delimits the irradiated membrane area with a diameter of 20 mm, equal to the UV transparent window in the module. As we will see later, an inhomogeneous light distribution will affect the overall conversion negatively compared to a homogeneous distribution at the same average UV light intensity.

Fig. 2 shows the light emission spectra for both lamps. The peak wavelength for the mono-LED lamp is at 366 nm and at 373 nm for the multi-LED lamp, where the full width half maximum (FWHM) is 10 nm for the mono-LED and 13 nm for the multi-LED. The energy generated from the mono-LED lamp corresponds to 3.39 eV and from the multi-LED lamp to 3.33 eV.

The synthesized TiO_2 layer on top of the membrane was predominantly composed of anatase (80–90%) and rutile crystal phases [28]. Both lamps irradiate above the energy gap for anatase and rutile marked in Fig. 2.

3.2. Irradiation effect on the discoloration of MB

Degradation experiments with methylene blue were conducted in a single-pass dead-end PMR, under light intensities between 50 to 550 W.m^{-2}. The normalized permeate concentration (c_p/c_b) as a function of the Péclet number (Pe $= uL/D$) is plotted together with fits based on Eq. (1) are shown in Fig. 3. For both membranes, the discoloration of MB increases with photon flux. For membrane A (Fig. 3a), the degree of discoloration at the lowest flow rate (1.6 L.m^{-2}.h^{-1}) with the mono-LED lamp was 56% for the lowest light intensity (50 W.m^{-2}), 66% for 100 W.m^{-2}, and 72% for 210 W m^{-2}, and with the multi-LED lamp was 87% for 350 W.m^{-2}, and 89% for the highest intensity (550 W.m^{-2}). Membrane B (Fig. 3b) displays very similar performance to membrane A, confirming the overall reproducibility of the method.

The lines in Fig. 3 represent Eq. (1) with the second Damköhler number obtained by least squares fitting of the experimental data accompanied with their 95% confidence intervals. The resulting surface reaction rate constants, k', are plotted as a function of the UV light intensity in Fig. 4, with the error bars representing their 95% confidence intervals.

Our experiments with the multi-LED lamp show a mostly linear increase of surface reaction rate constant with light intensity for the studied intensity range. Which corresponds to a reaction order $\beta \sim 1$ with respect to the incident photon flux. Conversely, the experiments with the mono-LED lamp show a deviation from linearity towards 210 W.m^{-2}, showing that the illumination distribution also affect the rate transition. Our model considers only the catalytic wall normal
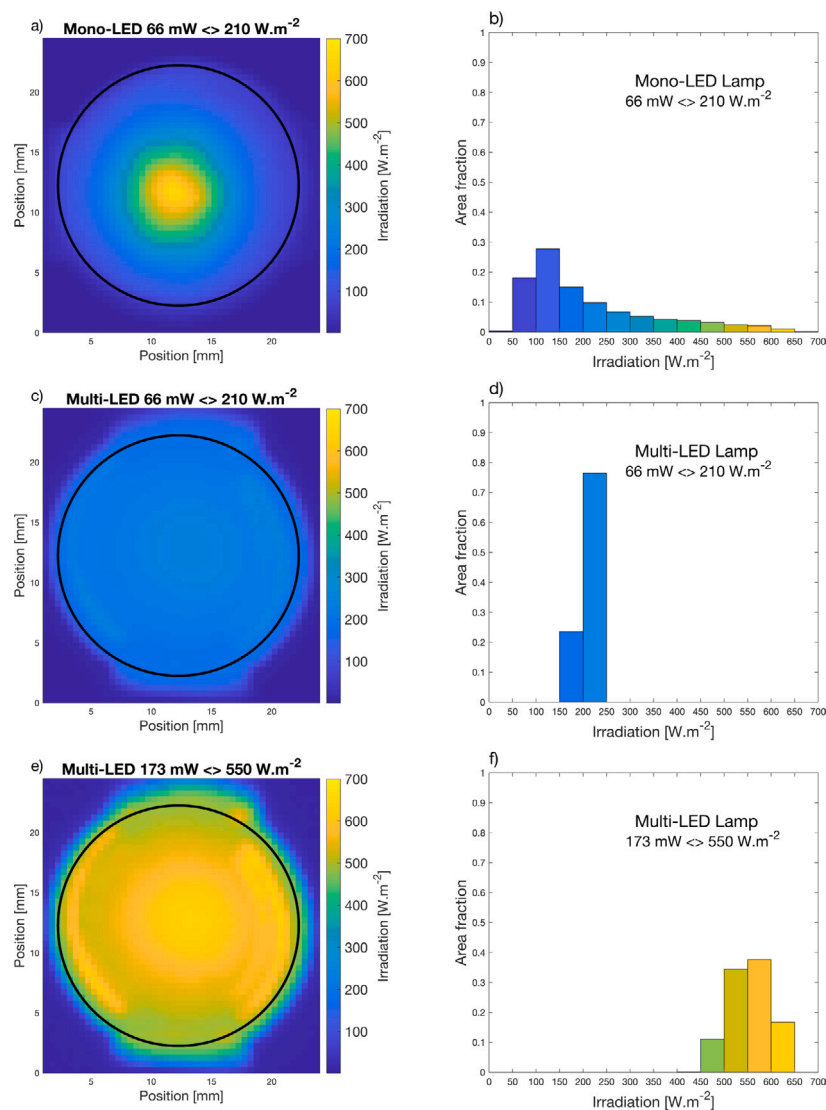
Fig. 1. Incident light irradiation distribution on the photocatalytic membrane (represented by the black circumference) and corresponding histograms indicating the area fraction per irradiation intensity. Figures (a) and (b) illustrate the data for the mono-LED lamp and (c), (d), (e), and (f) for the multi-LED lamp. The light sources were placed at a distance of 67 mm and 53 mm, respectively, from the membrane.

dimension and thus assumes a homogeneous irradiation distribution on the catalytic surface. This is clearly not the case for the mono-LED lamp, where a local maximum above 600 W.m^{-2} is observable in the center, see Fig. 1(a). Inhomogeneous radiation field distribution results in a lower overall conversion compared to homogeneously distributed light with equal average irradiation intensity. In our experiments, for the same light intensity and fluid flow, 210 W.m^{-2} and 9.7 L.m^{-2}.h^{-1}, we obtain 35% degradation with the mono-LED lamp and 55% degradation with the multi-LED lamp.

Using Eq. (1) we can compare, for example, the permeate concentration expected for Pe = 20 and Da$_{II}$ = 20 uniformly with that for Pe = 20 and having 30% surface with Da$_{II}$ = 60 and 70% surface with Da$_{II}$ = 2.85 (which corresponds to a surface average Da$_{II}$ = 20). In the homogeneous case, we would obtain a permeate concentration of 0.5, while in the inhomogeneous case, this is just 0.69. The results in Fig. 4 show that the differences in degradation between the mono and the multi-LED configuration are smaller at lower irradiation intensities. Using the same example as before, but in this case comparing Pe = 20 and Da$_{II}$ = 5 uniformly with Pe = 20 and having 30% surface with Da$_{II}$ = 3 and 70% surface with Da$_{II}$ = 0.14, we obtain a permeate concentration of 0.8 for the homogeneous case, while in the inhomogeneous case, this is 0.85. This highlights that the expected concentration differences

for the permeate due to inhomogeneous illumination distribution are less significant at lower overall light intensities. Note that in this theoretical example we assumed that Da$_{II}$ scales linearly with the light intensity. The inhomogeneous distribution can thus account for the reduced increase in conversion with increasing light intensity. This clearly demonstrates the importance of controlling the spatial light distribution when quantifying photocatalytic performance.

3.3. Photonic efficiency

The light utilization efficiency of the photoreactor can be assessed through the photonic efficiency, also known as apparent quantum yield or lower limit of the true quantum yield, which is expressed as the relation between the reaction rate [mol L^{-1} s^{-1}] and the photon flux [mol L^{-1} s^{-1}]. A rough estimation of the photon flux for monochromatic light can be calculated using the Planck relation (Appendix C). The membrane area irradiated by the lamp in our configuration is $\pi \cdot 10^{-4}$ m^2 and the reactor volume is $\pi \cdot 10^{-6}$ m^3. For our system, the calculated photonic efficiency, considering the methylene blue discoloration rate and the estimated photon flux, is 0.004 ± 0.002% for the mono-LED lamp and 0.0062 ± 0.0008% for the multi-LED lamp. The
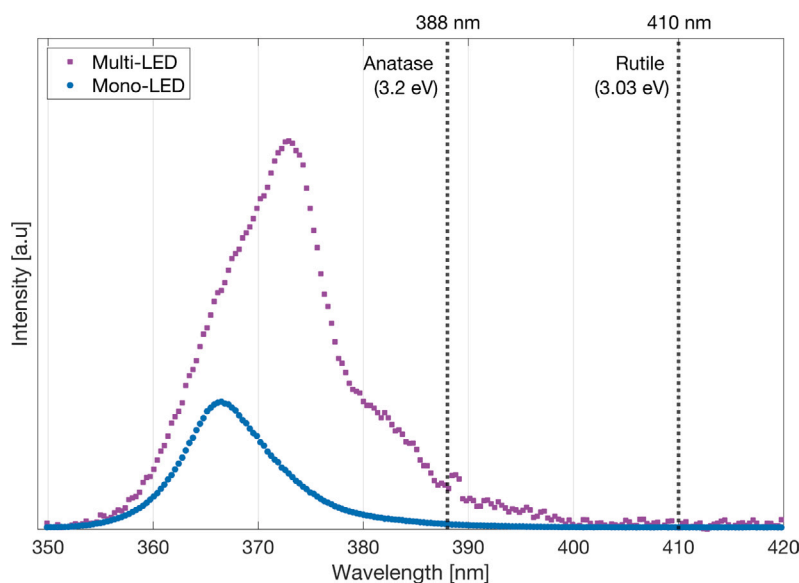
Fig. 2. Mono and multi-LED lamps spectra. The dashed lines mark the wavelength needed to overcome the energy gap of the anatase and rutile crystalline structures.
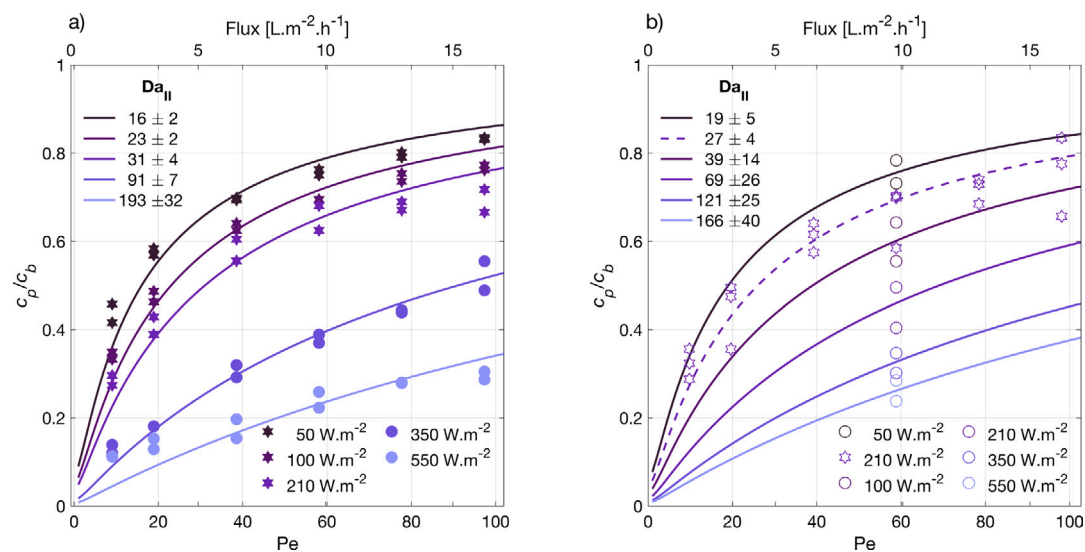

Fig. 3. Permeate to feed concentration ratio vs. filtration rate for different UV light intensities. The lines correspond to the mass transport and surface reaction model (Eq. (1)) with fitted second Damköhler number. Symbols depict the experimental data, where the stars show the experiments with the mono-LED lamp and the circles with the multi-LED lamp. Figure (a) shows the experiments with membrane A and Figure (b) the experiments with membrane B.

high electron–hole recombination rate causes the typically low quantum yield of photocatalytic reactions. Besides, the photonic efficiency considers the total incident amount of photons without considering light scattering or other effects. The most commonly reported quantum yield is calculated with the absorbed photons by the catalysts, which are around 65%. This maximum absorbed photons expectation was calculated by Rosenberg et al. [30] for a hollow glass microbead covered with a TiO$_2$. Furthermore, utilizing the discoloration of MB instead of the electron–hole formation or reactive oxygen species formed also translates into lower photonic efficiencies. The discoloration of MB is an indirect reaction with the incident photons since more reactions that we do not measure are possibly triggered.

Photon efficiency comparison with literature is difficult as most of the publications that report a quantum yield do not describe how the values are obtained, and there is no universally accepted approach to evaluate it [31]. The reported values are not more than a few percent and depend on the photocatalyst and experimental conditions [32]. Matthews [33] reported a quantum yield of 0.92% for the degradation

of methylene blue over thin films of TiO$_2$ assuming that the amount of photons absorbed by immobilized TiO$_2$ was the same as the amount of photons absorbed by the actinometer (potassium ferrioxalate). He used a 20 W NEC blacklight blue fluorescent tube (T10). Zhang et al. [34] described relative photonic efficiencies of 0.34% and 2.36% for the MB degradation in a slurry configuration for a high [5500–10000 W.m^{-2}] and low [4–20 W.m^{-2}] photon flux photocatalytic process respectively. They used a 250 W UV high pressure mercury lamp for the high photons fluxes and an 8 W black light lamp for the low photon flux and calculated the rate of incident photons reaching the reactor by actinometry.

3.4. Temperature effect

The temperature during the discoloration of methylene blue at different irradiation intensities was evaluated, and its effect is examined in this section. Fig. 5 depicts the temperature measured on top of the
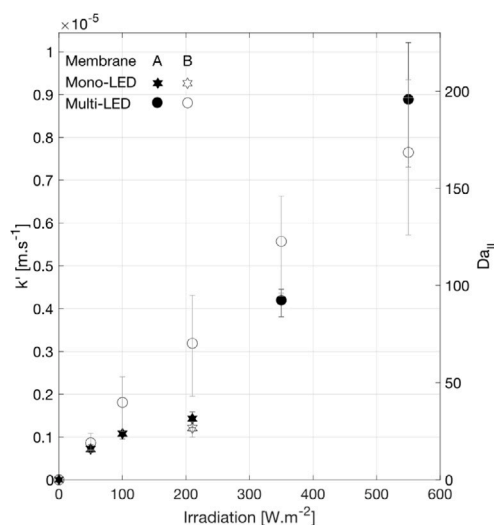
Fig. 4. Surface reaction rate constant and second Damköhler number as a function of the light intensity.
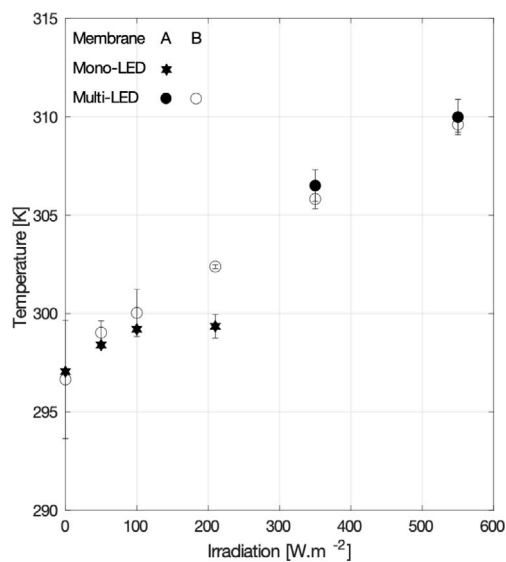

Fig. 5. Temperature as estimated from IR camera measurements as a function of the UV irradiation intensity.

Fig. A.6. PMR thermal image. Conditions: multi-LED lamp, 373 nm, 550 W.m^{-2}, and Pe = 59.

et al. [37], who reported a clear reduction in reaction rate of β-oestradiol with an increase of temperature for a range between 284 and 335 K. Similarly, Lair et al. [38] reported reduced naphthalene degradation with increasing temperature in a range from 283 to 313 K. Our experimental temperature range (299–310 K) may affect the dye adsorption–desorption on the photocatalytic surface but would only reduce the conversion at higher irradiation intensities.

4. Conclusion

The influence of light distribution on a photocatalytic membrane for the discoloration of methylene blue has been studied for different photon fluxes. A mono and a multi-LED lamp were used with a photocatalytic membrane reactor, and a detailed scan of their illumination profile was obtained and evaluated. The light intensity distribution influences the overall pollutant conversion, and its effect increases with the irradiation intensity. For a total irradiation on the membrane surface of 210 W.m^{-2}, and a filtration rate of 9.7 L.m^{-2}.h^{-1} the more homogeneous distribution improved the degradation from 35 to 55% compared to the inhomogeneous distribution. This clearly demonstrates the importance of controlling the illumination distribution when quantifying the photocatalytic performance. Furthermore, a surface reaction model that includes the mass transfer limitations was used to evaluate the surface reaction constant, and a linear relation with the photon flux was found for the homogeneous distribution in the studied range of irradiation intensities [50 to 550 W.m^{-2}], while for the nonuniform distribution a rate transition with respect to the incident photon flux was observed between 100 and 210 W.m^{-2}. This work adds valuable information on improving the light efficiency in a photoreactor to improve the degradation of pollutants. It also proves the importance of the light distribution when comparing studies, as for the same total irradiation, the outcome results will vary with the illumination distribution.

CRediT authorship contribution statement

Shuyana A. Heredia Deba: Writing – review & editing, Writing – original draft, Methodology, Investigation, Formal analysis, Data curation. **Bas A. Wols:** Writing – review & editing, Supervision, Methodology, Formal analysis, Conceptualization. **Doekle R. Yntema:** Writing

membrane during the experiments using an IR camera. The temperature difference from the lower irradiation intensity to the highest was around 11 degrees.

With the increase in temperature, a further increase in permeability (about 17% when accounting for the viscosity effect) was observed, suggesting that the actual temperature increase may be more significant than estimated from the IR camera. The difference in permeability did not affect the filtration rate as the syringe pump controlled the feed flows.

Photocatalytic systems are activated by photons and hence do not require heating. However, at high (>353 K) and very low (273 to 233 K) temperatures, the catalytic activity decreases [17]. In the medium temperature range (from 293 to 353 K), the apparent activation energy is often very small. Some researchers, such as Al-Sayyed et al. [35], and Terzian and Serpone [36], consider that thermally activated steps are negligible in this temperature range, i.e. the absorption/desorption processes are almost temperature-independent. The adsorption of micropollutants and intermediates on the catalyst surface typically improves with a decreased temperature. This is in agreement with Lotfi
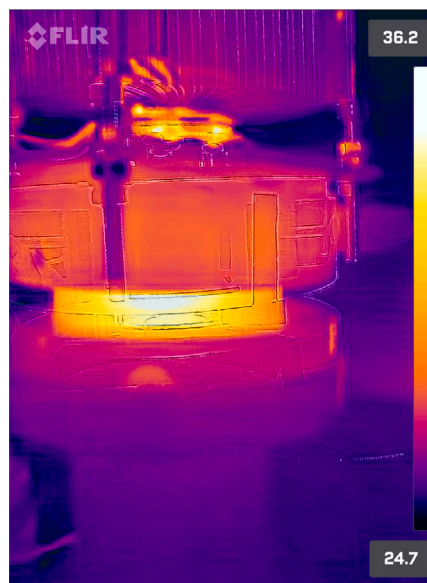
Table C.1
Photonic efficiencies of photocatalytic discoloration of MB under different photon fluxes.

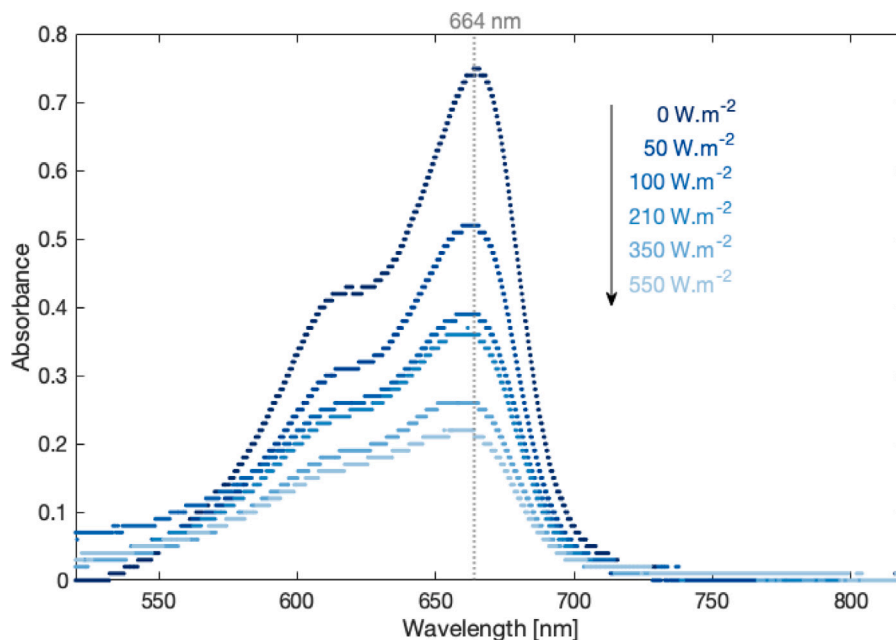| Membrane	LED lamp	k' [10^{-6} m s^{-1}]	Irradiation [W.m^{-2}]	Photon flux [10^{-7} mol.s^{-1}]	Photonic efficiency [%]
A	Mono	0.72	50	0.48	0.006
A	Mono	1.08	100	0.96	0.004
A	Mono	1.43	210	2.02	0.003
A	Multi	4.20	350	3.42	0.005
A	Multi	8.89	550	5.38	0.006
B	Mono	1.21	210	2.02	0.002
B	Multi	0.87	50	0.49	0.007
B	Multi	1.81	100	0.98	0.007
B	Multi	3.19	210	2.05	0.006
B	Multi	5.57	350	3.42	0.006
B	Multi	7.65	550	5.38	0.006

Fig. B.7. UV–Vis absorption spectra showing changes in methylene blue concentration at steady state under different irradiation intensities. Conditions: multi-LED lamp, 373 nm, Pe = 59.

– review & editing, Supervision, Investigation, Formal analysis, Data curation. **Rob G.H. Lammertink:** Writing – review & editing, Supervision, Project administration, Methodology, Investigation, Funding acquisition, Formal analysis, Conceptualization.

Declaration of competing interest

The authors declare that they have no known competing financial interests or personal relationships that could have appeared to influence the work reported in this paper.

Data availability

Data will be made available after acceptance/publication.

Appendix A. Temperature measurement

Fig. A.6 illustrates the temperature measurement image obtained with the thermal imaging camera FLIR ONE PRO for the experiment with the multi-LED lamp during the steady state with a flux of 9.7 L.m^{-2}.h^{-1} and an irradiation of 550 W.m^{-2}.

Appendix B. Methylene blue discoloration

The methylene blue discoloration was measured inline by a UV–Vis spectrometer. Fig. B.7 shows the permeate spectra at a steady state under the studied irradiation intensities for the second repetition of the experiments with the multi-LED lamp.

Control experiments were carried out with a membrane without the TiO$_2$ layer, and with an average irradiation of 210 W.m^{-2} to rule out effects other than the photocatalytic oxidation in the reaction with MB. We observed no significant removal of methylene blue, even at the lowest permeation rate.

Appendix C. Photonic efficiency

The energy carried by a photon, E [J photon^{-1}], is directly proportional to the electromagnetic frequency of the photon and hence, it is inversely proportional to the wavelength, λ. This energy is expressed by the Planck relation:

$$E = \frac{hc}{\lambda} \qquad (C.1)$$

where h is the Planck's constant (6.626×10^{-34} J.s), c is the speed of light (3×10^8 m.s^{-1}), and λ is the wavelength of the lamp (366×10^{-9} m for the mono-LED or 373×10^{-9} m for the multi-LED). Using the Avogadro's number (6.022×10^{23} mol^{-1}) it is possible to calculate the energy per mol of photons. Hence, the photon energy from the mono-LED lamp in our system is 3.27×10^5 J.mol^{-1} and 3.21×10^5 J.mol^{-1} for the multi-LED lamp. For an irradiation of 1 W it is equal to 3.06×10^{-6} mol.s^{-1} for the mono-LED lamp and 3.11×10^{-6} mol.s^{-1} for the multi-LED lamp. Table C.1 summarizes the photonic efficiencies calculations of photocatalytic discoloration of MB for each experiment. The photonic efficiency slightly decreases with the increasing illumination because the recombination of electron–hole pairs is enhanced at higher irradiation intensities.

References

[1] M.E. Leblebici, G.D. Stefanidis, T. Van Gerven, Comparison of photocatalytic space-time yields of 12 reactor designs for wastewater treatment, Chem. Eng. Process.: Process Intensif. 97 (2015) 106–111.

[2] C. Casado, R. Timmers, A. Sergejevs, C. Clarke, D. Allsopp, C. Bowen, R. van Grieken, J. Marugán, Design and validation of a LED-based high intensity photocatalytic reactor for quantifying activity measurements, Chem. Eng. J. 327 (2017) 1043–1055.

[3] X. Li, Y. Chen, Y. Tao, L. Shen, Z. Xu, Z. Bian, H. Li, Challenges of Photocatalysis and Their Coping Strategies, Chem Catalysis, 2022.

[4] L.G. Devi, R. Kavitha, A review on non metal ion doped titania for the photocatalytic degradation of organic pollutants under UV/solar light: Role of photogenerated charge carrier dynamics in enhancing the activity, Appl. Catal. B 140–141 (2013) 559–587.

[5] Y.-Y. Wang, Y.-X. Chen, T. Barakat, Y.-J. Zeng, J. Liu, S. Siffert, B.-L. Su, Recent advances in non-metal doped titania for solar-driven photocatalytic/photoelectrochemical water-splitting, J. Energy Chem. 66 (2022) 529–559.

[6] S.Y. Chai, Y.J. Kim, W.I. Lee, Photocatalytic WO3/TiO2 nanoparticles working under visible light, J. Electroceram. 17 (2) (2006) 909–912.

[7] S. Rtimi, R. Sanjines, C. Pulgarin, A. Houas, J.-C. Lavanchy, J. Kiwi, Coupling of narrow and wide band-gap semiconductors on uniform films active in bacterial disinfection under low intensity visible light: Implications of the interfacial charge transfer (IFCT), J. Hard Mater. 260 (2013) 860–868.

[8] S. Ghafoor, S. Ata, N. Mahmood, S.N. Arshad, Photosensitization of TiO2 nanofibers by Ag2S with the synergistic effect of excess surface Ti3+ states for enhanced photocatalytic activity under simulated sunlight, Sci. Rep. 7 (1) (2017) 255.

[9] J.P. Ghosh, C.H. Langford, G. Achari, Characterization of an LED based photoreactor to degrade 4-chlorophenol in an aqueous medium using coumarin (c-343) sensitized TiO2, J. Phys. Chem. A 112 (41) (2008) 10310–10314.

[10] L.H. Levine, J.T. Richards, J.L. Coutts, R. Soler, F. Maxik, R.M. Wheeler, Feasibility of ultraviolet-light-emitting diodes as an alternative light source for photocatalysis, J. Air Waste Manag. Assoc. 61 (9) (2011) 932–940.

[11] A. Fujishima, K. Honda, Electrochemical photolysis of water at a semiconductor electrode, Nature 238 (5358) (1972) 37–38.

[12] I. Izumi, W.W. Dunn, K.O. Wilbourn, F.-R.F. Fan, A.J. Bard, Heterogeneous photocatalytic oxidation of hydrocarbons on platinized titanium dioxide powders, J. Phys. Chem. 84 (24) (1980) 3207–3210.

[13] D.F. Ollis, E. Pelizzetti, N. Serpone, Photocatalyzed destruction of water contaminants, Environ. Sci. Technol. 25 (9) (1991) 1522–1529.

[14] T.A. Egerton, C.J. King, The influence of light intensity on photoactivity in TiO2 pigmented systems, J. Oil Colour Chem. Assoc. 62 (1979) 386–391.

[15] M.R. Hoffmann, S.T. Martin, W. Choi, D.W. Bahnemann, Environmental applications of semiconductor photocatalysis, Chem. Rev. 95 (1) (1995) 69–96.

[16] J.-M. Herrmann, Heterogeneous photocatalysis: Fundamentals and applications to the removal of various types of aqueous pollutants, Catal. Today 53 (1) (1999) 115–129.

[17] J.-M. Herrmann, Heterogeneous photocatalysis: state of the art and present applications, Top. Catalysis 34 (2005) 49–65.

[18] R. Lyubimenko, D. Busko, B.S. Richards, A. Schäfer, A. Turshatov, Efficient photocatalytic removal of methylene blue using a metalloporphyrin–poly(vinylidene fluoride) hybrid membrane in a flow-through reactor, ACS Appl. Mater. Interfaces 11 (35) (2019) 31763–31776.

[19] D.F. Ollis, Solar-assisted photocatalysis for water purification: Issues, data, questions, in: E. Pelizzetti, M. Schiavello (Eds.), Photochemical Conversion and Storage of Solar Energy, Springer, Dordrecht, Netherlands, 1991, pp. 593–622.

[20] M. Aguado, M. Anderson, C. Hill, Influence of light intensity and membrane properties on the photocatalytic degradation of formic acid over TiO2 ceramic membranes, J. Mol. Catal. 89 (1) (1994) 165–178.

[21] Z. Wang, J. Liu, Y. Dai, W. Dong, S. Zhang, J. Chen, Dimethyl sulfide photocatalytic degradation in a light-emitting-diode continuous reactor: Kinetic and mechanistic study, Ind. Eng. Chem. Res. 50 (13) (2011) 7977–7984.

[22] P.C.K. Vesborg, S.-i. In, J.L. Olsen, T.R. Henriksen, B.L. Abrams, Y. Hou, A. Kleiman-Shwarscstein, O. Hansen, I. Chorkendorff, Quantitative measurements of photocatalytic CO-oxidation as a function of light intensity and wavelength over TiO2 nanotube thin films in μ-reactors, J. Phys. Chem. C 114 (25) (2010) 11162–11168.

[23] A. Visan, D. Rafieian, W. Ogieglo, R.G.H. Lammertink, Modeling intrinsic kinetics in immobilized photocatalytic microreactors, Appl. Catal. B 150–151 (2014) 93–100.

[24] N.A. Timmerhuis, J.A. Wood, R.G. Lammertink, Connecting experimental degradation kinetics to theoretical models for photocatalytic reactors: The influence of mass transport limitations, Chem. Eng. Sci. 245 (2021) 116835.

[25] A. Visan, J.R. Van Ommen, M.T. Kreutzer, R.G. Lammertink, Photocatalytic reactor design: Guidelines for kinetic investigation, Ind. Eng. Chem. Res. 58 (2019) 5349–5357.

[26] M. Martín-Sómer, C. Pablos, R.V. Grieken, J. Marugán, Influence of light distribution on the performance of photocatalytic reactors: LED vs mercury lamps, Appl. Catal. B 215 (2017) 1–7.

[27] F. Khodadadian, A. Poursaeidesfahani, Z. Li, J.R. van Ommen, A.I. Stankiewicz, R. Lakerveld, Model-based optimization of a photocatalytic reactor with light-emitting diodes, Chem. Eng. Technol. 39 (10) (2016) 1946–1954.

[28] S.A. Heredia Deba, B.A. Wols, D.R. Yntema, R.G. Lammertink, Transport and surface reaction model of a photocatalytic membrane during the radical filtration of methylene blue, Chem. Eng. Sci. 254 (2022) 117617.

[29] ANSYS Fluent Theory Guide, ANSYS Inc., 2013.

[30] I. Rosenberg, J. Brock, A. Heller, Collection optics of titanium dioxide photocatalyst on hollow glass microbeads floating on oil slicks, J. Phys. Chem. 96 (8) (1992) 3423–3428.

[31] V. Pareek, S. Chong, M. Tadé, A.A. Adesina, Light intensity distribution in heterogenous photocatalytic reactors, Asia-Pac. J. Chem. Eng. 3 (2) (2008) 171–201.

[32] S.K. Loeb, P.J. Alvarez, J.A. Brame, E.L. Cates, W. Choi, J. Crittenden, D.D. Dionysiou, Q. Li, G. Li-Puma, X. Quan, D.L. Sedlak, T. David Waite, P. Westerhoff, J.-H. Kim, The technology horizon for photocatalytic water treatment: Sunrise or sunset? Environ. Sci. Technol. 53 (6) (2019) 2937–2947.

[33] R.W. Matthews, Photocatalytic oxidation and adsorption of methylene blue on thin films of near-ultraviolet-illuminated TiO2, J. Chem. Soc. Faraday Trans. 1: Phys. Chem. Condens. Phases 85 (6) (1989) 1291–1302.

[34] Q. Zhang, C. Li, T. Li, Rapid photocatalytic degradation of methylene blue under high photon flux UV irradiation: Characteristics and comparison with routine low photon flux, Int. J. Photoenergy 2012 (2012) 398787.

[35] G. Al-Sayyed, J.-C. D'Oliveira, P. Pichat, Semiconductor-sensitized photodegradation of 4-chlorophenol in water, J. Photochem. Photobiol. A 58 (1) (1991) 99–114.

[36] R. Terzian, N. Serpone, Heterogeneous photocatalyzed oxidation of creosote components: mineralization of xylenols by illuminated TiO2 in oxygenated aqueous media, J. Photochem. Photobiol. A 89 (2) (1995) 163–175.

[37] S. Lotfi, K. Fischer, A. Schulze, A. Schäfer, Photocatalytic degradation of steroid hormone micropollutants by TiO2-coated polyethersulfone membranes in a continuous flow-through process, Nature Nanotechnol. 17 (2022) 417–423.

[38] A. Lair, C. Ferronato, J.-M. Chovelon, J.-M. Herrmann, Naphthalene degradation in water by heterogeneous photocatalysis: An investigation of the influence of inorganic anions, J. Photochem. Photobiol. A 193 (2) (2008) 193–203.